Magnetoplasmons in high electron mobility CdTe/CdMgTe quantum wells

I. Grigelionis,[1,*] K. Nogajewski,[1,†] G. Karczewski,[2] T. Wojtowicz,[2] M. Czapkiewicz,[2] J. Wróbel,[2,3] H. Boukari,[4,5] H. Mariette,[4,5] and J. Łusakowski[1]

[1]*Faculty of Physics, University of Warsaw, ul. Pasteura 5, PL-02-093 Warsaw, Poland*

[2]*Institute of Physics, PAS, al. Lotników 32/46, PL-02-668 Warsaw, Poland*

[3]*Faculty of Mathematics and Natural Sciences, Rzeszów University, al. Rejtana 16C, PL-35-959 Rzeszów, Poland*

[4]*University of Grenoble Alpes, Institute Néel, F-38042 Grenoble, France*

[5]*CNRS, Institute Néel, F-38042 Grenoble, France*

(Received 30 October 2014; revised manuscript received 3 February 2015; published 24 February 2015)

Terahertz magnetospectroscopy experiments on high quality CdTe/CdMgTe quantum wells were carried out at low temperatures and high magnetic fields. Samples of two different geometries were considered: a large-area grid-gated sample and a split-gate quantum point contact (QPC). The spectra show features originating from a cyclotron resonance transition and magnetoplasmon excitations. Depending on the sample geometry, plasmons characterized by an effective dielectric function of a mixed gated/ungated (in grid-gated samples) or ungated type (in the QPC) were excited. In each case, the resulting plasmon dispersion relation was determined and we show that it can be precisely described within a theory based on a local approximation of a high-frequency magnetoconductivity tensor of a two-dimensional electron gas by taking into account a polaron effect and plasmon-longitudinal optical (LO) phonon interaction.

DOI: 10.1103/PhysRevB.91.075424 PACS number(s): 71.45.Gm, 78.30.Fs, 78.67.De

I. INTRODUCTION

Excitation of charge density oscillations in an electron plasma (plasmons) has been a topic of intense research in solid state physics. Plasmons in two dimensions (2D) are of a special interest as their frequency ω depends on the wave vector k, which allows for a better control of the excitation spectrum, as has already been demonstrated by experimental works on inversion layers in Si [1–4] and quantum wells based on GaAs [5–7], InGaAs [8,9], or GaN [10–12]. There are two main factors determining the quantization of plasmon wave vectors. First, they can be quantized by the period of a metallic grid (or other periodic structure) deposited above a 2D plasma. In such systems, the incident radiation diffracts on the grid and generates waves which carry an in-plane momentum large enough to excite plasmons. If the period of the grid is Λ, then the wave vectors of the excited plasmons are $k_j = 2\pi j/\Lambda$, with an integer j. Let us note that the idea of using periodic systems to couple photons with plasmons was realized in different ways [1,3,7]. Second, it was shown in many experiments that the plasmon wave vector can be defined by the details of the sample geometry, in particular, by the sample's width W [4,13–17]. If the sample is symmetrical and the radiation power uniformly distributed, then, due to the symmetry of the problem, $k_j = (2j-1)\pi/W$, which means that only plasmons with an odd number of halves of the wavelength can be excited [14]. In general, however, all modes can be excited and observed [17]. It was shown recently in Refs. [18,19] that, depending on the frequency of the THz radiation and the gate geometry, in the same sample one can excite plasmons with k vectors defined either by the width of the mesa or the period of the grid.

Recently, high quality CdTe/CdMgTe and CdMnTe/CdMgTe quantum wells were used in a number of advanced experiments. Resistance quantization in a quantum point contact (QPC) [20], a fractional quantum Hall effect [21], as well as spin current effects [22,23] were studied. Excitation of THz radiation induced by optically generated spin waves in CdMnTe/CdMgTe containing a high-mobility 2D electron plasma was demonstrated [24]. Also, there are a few reports on a THz spectroscopy in these systems. The cyclotron resonance was investigated, the electron cyclotron mass was determined, and a polaron effect was observed in modulation doped CdTe/CdMgTe quantum wells of different widths [25,26]. The electron cyclotron mass was also determined in nominally undoped CdTe/CdMnTe quantum wells of different widths using the optically detected cyclotron resonance technique [27], and a good agreement with the results on the electron cyclotron mass presented in Ref. [26] was found. Collective excitations of a 2D magnetoplasma were reported in a Raman spectroscopy experiment on modulation doped CdTe/CdMnTe QWs [28]. Also, an impurity shifted cyclotron resonance was reported in Ref. [25] and shallow impurity transitions in CdTe/CdMgTe quantum wells continuously doped with iodine were studied [29,30].

In this paper we report on the results of THz magnetospectroscopy experiments carried out on grid-gated samples and a quantum point contact processed on wafers with a single modulation doped CdTe/CdMgTe quantum well. The main result is the direct observation of magnetoplasmon excitations in CdTe/CdMgTe quantum wells in a far-infrared magnetospectroscopy experiment and a description of the resulting dispersion relation within a theoretical model. We have found that in the case of grid-gated samples, the $\omega(k)$ relation is precisely described by plasmon resonances of a mixed type, i.e., intermediate between the gated and ungated plasmons, with their wave vector quantized according to the

*ignas.grigelionis@fuw.edu.pl

†Current address: Laboratoire National des Champs Magnétiques Intenses, CNRS-UJF-UPS-INSA, 25, rue des Martyrs, 38042 Grenoble, France.

period of the grid. In the case of the QPC, a dispersion of ungated plasmons was found with the wave vector defined by the dimensions of the mesa. We show that corrections must be taken into account in plasmon dispersion, which result from a strong electron-phonon and plasmon-phonon interaction in CdTe.

II. SAMPLES AND EXPERIMENT

The investigated samples consist of a single CdTe/CdMgTe quantum well grown by molecular beam epitaxy on 2-in. GaAs(100) wafers. Iodine n-type modulation doping is introduced in the top CdMgTe barrier [Figs. 1(a) and 1(c)]. Three samples were processed out of the same wafer with a sheet electron concentration $n_s = 3.0 \times 10^{11}$ cm^{-2} and mobility $\mu = 2.6 \times 10^5$ cm^2/V s, determined by Hall effect measurements at $T = 1.4$ K. Photolithography and aluminum lift-off allowed to define a 1.6 mm $\times$ 1.6 mm grid coupler [Fig. 1(b)] isolated from the surface of the wafer by a 70-nm-thick SiO_2 layer. The coupler period Λ was equal to 2 and 3 μm for samples G1 and G2, respectively, and the geometrical aspect ratio of the grid was equal to 50% in each case. A reference sample GR was prepared with neither a grid nor a SiO_2 layer.

The QPC [Fig. 1(d)] was realized by electron beam lithography on a wafer with a sheet electron concentration

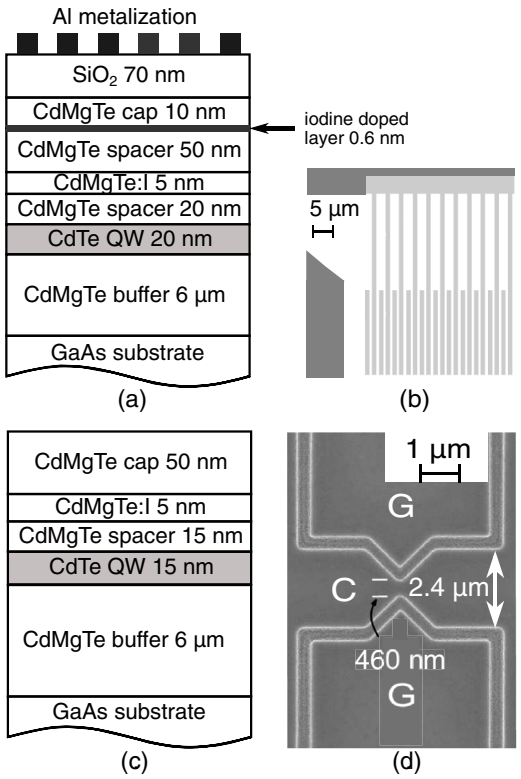

FIG. 1. (Color online) A layout of wafers used for the fabrication of (a) the grid-gated samples and (c) a quantum point contact. (b) shows a sketch of a metallic grid pattern, lithographically defined on the wafer surface. A scanning electron microscope picture of the quantum point contact device is presented in (d), showing a split gate (G) and a conduction channel (C).

equal to $n_s = 5.2 \times 10^{11}$ cm^{-2} and a mobility equal to $\mu = 2.3 \times 10^5$ cm^2/V s at $T = 1.8$ K. Etched grooves separate the channel (C) from two lateral gates (G). The nominal width of the channel W is equal to 2.4 μm and decreases to 460 nm at the narrowest part. Ohmic contacts were formed by soldering indium. More details on the QPC sample preparation and its electrical characterization can be found elsewhere [20].

THz magnetospectroscopy experiments were performed in the Faraday configuration, at a temperature $T = 1.8$ K and magnetic fields B up to 12 T. THz radiation from an optically pumped THz laser operating on methanol in the cw mode was mechanically modulated and guided to the sample through an oversized metallic waveguide. Transmission spectra on the grid-gated and reference samples were collected by a carbon bolometer. The sample was permanently illuminated with a white light during the transmission measurements. It was observed that, without a visible light irradiation, the cyclotron resonance as well as magnetoplasma resonance peaks did not show up at all, being hidden in the noise level. We suppose that it was due to the fact that the quality and/or concentration of the two-dimensional electron gas (2DEG) in the samples was deteriorated as a result of the top metallization deposited on the sample and other lithography steps. The concentration of electrons which we have found in samples illuminated with a visible light was 3.2×10^{11} cm^{-2}, just slightly above that measured on an unprocessed wafer in the dark (3.0×10^{11} cm^{-2}). This allows us to treat both illuminated and not illuminated reference samples on equal footing.

Photocurrent spectra on the quantum point contact were recorded by measurements of a voltage drop on a resistor connected in series with the sample. Both transmission and photocurrent spectra were measured as a function of B with a lock-in technique.

III. RESULTS AND DISCUSSION

The transmission spectra measured at laser frequencies of 2.52 and 3.11 THz on samples G1, G2, and GR are shown in Fig. 2(a). The position of a deep minimum visible in each spectrum corresponds to the cyclotron resonance (CR) transition. The cyclotron effective mass $m_c^* = (0.1008 \pm 0.0005)m_e$ determined for this 20-nm-thick CdTe quantum well at $B \sim 9.1$ T is in a close agreement with the value obtained by Karczewski *et al.* [26]. For magnetic fields around 11.5 T we observe a higher cyclotron effective mass $m_c^* = (0.1029 \pm 0.0005)m_e$; this increase is due to a polaron effect [31]. A comparison of the spectra in Fig. 2(a) clearly shows a symmetrical CR line shape for the sample GR and a few dips (marked with triangles) on a low-B shoulder of the CR minimum in the case of samples G1 and G2. We interpret them as features resulting from the excitation of the fundamental and three subsequent magnetoplasmon modes.

In order to find the full width at half maximum (FWHM) of the magnetoplasmon and CR peaks, the baseline was subtracted and the procedure of deconvolution to Lorentzian peaks was performed on spectra (c) (sample G2) and (d) (sample G1). The results are shown in Fig. 2 by dotted lines. An average FWHM of magnetoplasmon peaks [0.10 and 0.16 T for (c) and (d), respectively] was found to be very close to that of

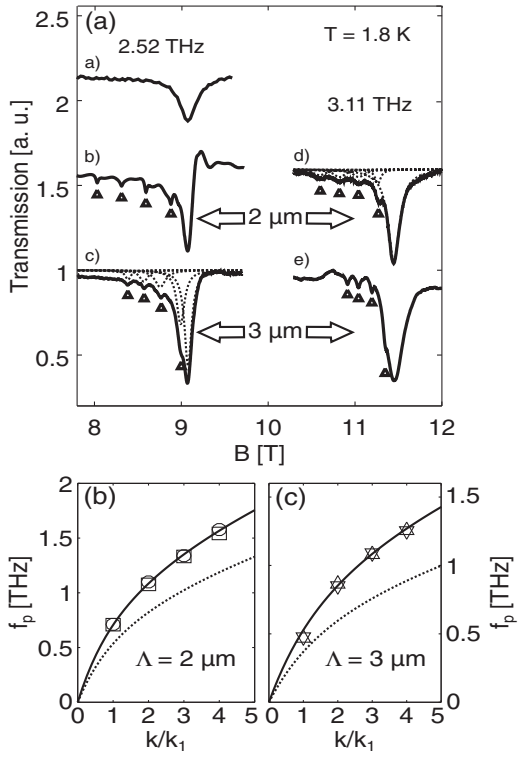

FIG. 2. (a) Transmission dependence on the magnetic field for samples GR [no grid, curve (a)], G1 [$\Lambda = 2$ μm, curves (b) and (c)], and G2 $\Lambda = 3$ μm, curves (d) and (e)] at laser frequencies of 2.52 and 3.11 THz. Triangles mark the peaks of the magnetoplasma resonances. Lorentzians resulting from the deconvolution procedure on curves (c) and (d) are represented by dotted lines. Squares and circles in (b): Experimental plasmon dispersion for $\Lambda = 2$ and 3 μm, respectively, at 2.52 THz. Up (down) triangles in (c): Experimental plasmon dispersion for $\Lambda = 2$ μm ($\lambda = 3$ μm) at 3.11 THz. Solid (dotted) lines in (b) and (c): Theoretical plasmon dispersion [Eq. (3)] with (without) a plasmon-LO phonon interaction.

the CR peak (0.10 and 0.14 T), which suggests that, in general, they are approximately equal to each other. The width of the resonances in sample G2 is higher by approximately 50% than in sample G1. This could result from different patterns of the scattering centers in these two samples cooled separately in different experimental runs.

In the presence of an external magnetic field perpendicular to a 2D electron plane, plasmons couple to the electron cyclotron motion and form hybrid resonant excitations—magnetoplasmons. In general, a description of magnetoplasmons should be carried out within a nonlocal model of the magnetoconductivity tensor of an electron gas, which leads to the following dispersion relation of 2D magnetoplasma oscillations [32]:

$$\frac{\omega^2-\omega_{\rm LO}^2}{\omega^2-\omega_{\rm TO}^2}-\frac{\omega_{p,j}^2}{X_j^2}\sum_{l=1}^{\infty}\frac{4l^2J_l^2(X_j)}{\omega^2-(l\omega_c)^2}=0. \tag{1}$$

In the expression above, $J_l(X_j)$ represents the Bessel function of the first kind and order l, and $X_j = 2\pi r_c/\lambda_j$ ($j = 1,2,3,\ldots$) is a so-called nonlocal parameter that quantifies the extent to which the wavelength of a given plasmon mode $\lambda_j = 2\pi/k_j$ matches the cyclotron radius r_c; $\omega_{p,j}$ and ω_c are the 2D plasmon and cyclotron frequencies, respectively. For completeness, a derivation of Eq. (1) is given in the Appendix. The first term on the left-hand side of Eq. (1) results from a plasmon-longitudinal optical (LO) phonon coupling [33], which plays an important role in polar semiconductors. The frequencies of transverse and longitudinal optical phonons in bulk CdTe are $\omega_{\rm TO} = 2\pi c\,\widetilde{\nu}_{\rm TO}$ and $\omega_{\rm LO} = 2\pi c\,\widetilde{\nu}_{\rm LO}$, with $\widetilde{\nu}_{\rm TO} = 140.10$ cm^{-1}, $\widetilde{\nu}_{\rm LO} = 169.45$ cm^{-1} (c is the speed of light).

For a small or large X_j (at high or low magnetic fields or for plasma oscillations of sufficiently long wavelengths) a local approximation of Eq. (1) can be used:

$$\frac{\omega^2-\omega_{\rm LO}^2}{\omega^2-\omega_{\rm TO}^2}-\frac{\omega_{p,j}^2}{\omega^2-\omega_c^2}\backsimeq 0. \tag{2}$$

The range of its validity is material dependent and can only be determined by solving Eq. (1) to find a range of X_j where nonlocal effects are negligible (see below). An expression for $\omega_{p,j}$ in the long-wavelength limit reads [34]

$$\omega_{p,j}^2=\frac{n_s e^2 k_j}{2\bar{\varepsilon}(k_j,d)\varepsilon_0 m^*}, \tag{3}$$

where n_s is the electron sheet density, k_j is the wave vector of the jth plasmon mode ($j = 1,2,3,\ldots$), $\bar{\varepsilon}$ is an effective dielectric function, and m^* is an electron effective mass. In calculations we took m^* equal to the cyclotron effective mass, including the polaron effect as determined in Ref. [31].

Effective dielectric functions for gated and ungated plasmons are expressed as $\bar{\varepsilon}_g(k_j,d) = 1/2[\varepsilon_s + \varepsilon_b \coth(k_j d)]$ and $\bar{\varepsilon}_{ug}(k_j,d) = 1/2\,\{\varepsilon_s + \varepsilon_b[1 + \varepsilon_b \tanh(k_j d)]/[\varepsilon_b + \tanh(k_j d)]\}$, respectively [35], where ε_s is the static dielectric constant of the quantum well, ε_b is the static dielectric constant of the barrier, and d is the barrier thickness. However, if $\varepsilon_b \gg 1$, the dielectric function for ungated plasmons can be approximated as $\bar{\varepsilon}_{ug}(k_j,d) = 1/2[\varepsilon_s + \varepsilon_b \tanh(k_j d)]$. Considering $\varepsilon_b \approx 10$ (a typical value for a CdTe-based semiconductor), such an approximation gives an error within 2% for the highest plasmon harmonics observed—fourth and 12th in grid-gated and QPC samples, respectively. When the plasmon-LO phonon interaction is considered, the static dielectric constants in the expressions for $\bar{\varepsilon}_g(k_j,d)$ and $\bar{\varepsilon}_{ug}(k_j,d)$ are replaced with their high-frequency counterparts $\varepsilon_{\infty,s}$ and $\varepsilon_{\infty,b}$ (see the Appendix), which was done in the present calculations.

In general, gated plasmons localized under metallic fingers of the grid form mixed modes with ungated plasmons existing in the grid's openings. It has been recently shown for a GaAs/AlGaAs [18] and GaN/AlGaN [32] heterostructures that a very good phenomenological description of these modes can be obtained with an effective dielectric function approximated by a weighted average of effective dielectric functions for the gated, $\bar{\varepsilon}_g$, and ungated, $\bar{\varepsilon}_{ug}$, cases,

$$\bar{\varepsilon} = (1-\alpha)\bar{\varepsilon}_g + \alpha\bar{\varepsilon}_{ug}, \tag{4}$$

where $0 \leqslant \alpha \leqslant 1$ is the weighting parameter.

Equation (2) was used to transform the positions of magnetoplasmon resonances in the magnetic field to plasmon frequencies. The plasmon wave vector $k_j = 2\pi j/\Lambda$ is quantized according to the grid period Λ. The inset in Fig. 2

shows experimental plasmon frequencies for the grid periods of 2 μm (squares, 2.52 THz; circles, 3.11 THz) and 3 μm (up triangles, 2.52 THz; down triangles, 3.11 THz), as a function of the normalized wave vector k/k_1, where $k_1 = 2\pi/\Lambda$. Solid lines are fits of Eq. (3) with an effective dielectric function described by Eq. (4) and with fitting parameters $\alpha = 0.45$ (close to the geometrical aspect ratio of the grid) and $\varepsilon_{b,\infty} = 5.9$ (below the value of a high-frequency dielectric constant of bulk CdTe, $\varepsilon_\infty = 7.1$; this lower value can result from a complex structure of the barrier that comprises, in particular, an SiO_2 layer, with its $\varepsilon = 3.9$). The dotted curves in Figs. 2(b) and 2(c) represent the plasmon dispersion when the plasmon-LO phonon interaction is neglected, calculated according to Eqs. (3) and (4), with $\alpha = 0.45$ and using the values of static dielectric constants ε_s and ε_b to evaluate $\bar{\varepsilon}_g(k_j,d)$ and $\bar{\varepsilon}_{ug}(k_j,d)$. As it can be seen, it gives a frequency lower by about 30% than in the case when a plasmon-LO phonon coupling is included in the calculations and $\varepsilon_{\infty,s}$ and $\varepsilon_{\infty,b}$ are used. The value of α highlights the mixed nature of the excited magnetoplasma waves, which—propagating through both gated and ungated regions of a 2D electron gas—are screened by the grid in a complicated manner.

For the highest mode ($j = 4$) observed at 2.52 THz, the calculated values of the nonlocal parameter X_4 are 0.14 and 0.11 (0.11 and 0.07 at 3.11 THz) for samples G1 and G2, respectively. As can be shown using Eq. (1), the values of X_4 below which no significant influence of nonlocal effects on the dispersion relation should be seen are equal to about 0.28 for G1 and about 0.19 for G2. This explains why the experimental results obtained on both grid-gated structures can be described by Eq. (2), i.e., in a local approximation.

The photocurrent spectra $P = P(B)$ of the QPC excited by the THz laser at a frequency equal to 2.52 THz are shown in Fig. 3(a) for a few different voltages V_g that were symmetrically applied to the lateral gates. The value of the effective mass found from the position of the CR maxima is equal to $(0.1028 \pm 0.0005)m_e$ in a 15-nm-wide CdTe/CdMgTe quantum well, and agrees with an estimation given in Ref. [26]. A series of spectral features accompanying the CR peak represents magnetoplasmon modes starting from the fundamental one up to its 12th harmonics. The structure was decomposed to Lorentzians [shown by a dotted line in Fig. 3(a)]. The FHWM of CR and magnetoplasmon peaks was found to be the same and equal to 0.32 T, much larger than that found for grid-gated samples. We think that it is the disorder at the etched mesa borders that results in this broadening since, in the case of the QPC, the magnetoplasmons are defined by the mesa width.

A set of plasmon frequencies derived from their magnetic-field positions is displayed with open circles in Fig. 3(b). Drawn with a solid line is the dispersion for ungated plasma oscillations confined in the channel of the device that was fitted to the experimental data using the same approach as in the case of the grid-gated samples but with the wavelength of the fundamental mode equal to the channel width $W = 2.4$ μm. The obtained fitting parameters are $\alpha = 0.95$ and $\varepsilon_b = 6.3$. The dispersion for the case when plasmon-LO photon coupling is excluded is shown by a dashed line. Here, similarly to the case of the grid-gate sample, it also gives a plasmon frequency that is lower by approximately 30%. The magnetoplasmon resonances are practically ungated and a residual screening

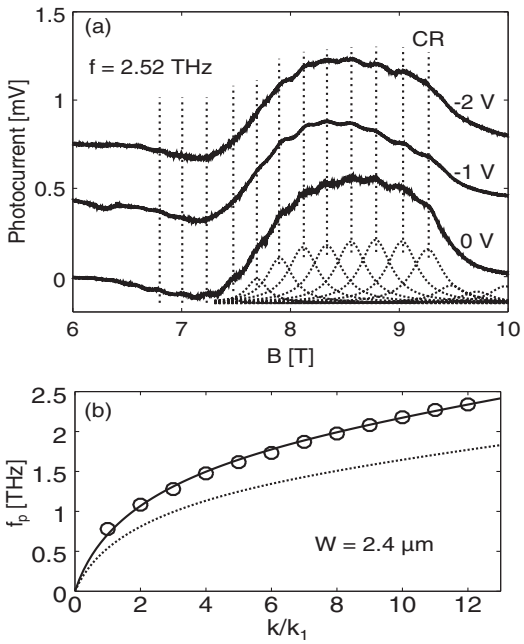

FIG. 3. (a) Photocurrent signal recorded on the QPC at different V_g. Spectra are shifted vertically for clarity. Vertical lines are guides to the eye to mark the positions of the maxima in the spectra. The cyclotron resonance position is denoted by CR. Deconvolution to Lorentzians is shown (dotted curves) for a spectrum measured at $V_g = 0$ V. (b) Experimental frequencies of the plasmon modes (open circles) fitted with a theoretical dispersion relation including a plasmon-LO phonon interaction (solid curve) and neglecting it (dotted curve).

they experience most probably results from the presence of the lateral gates. Here, the local approximation [Eq. (2)] provides a good description of the plasmon dispersion, even if the parameter X reaches values as high as 0.25 for the highest mode. According to the estimation based on Eq. (1), however, at a radiation frequency of 2.52 THz, the dispersion relation of the magnetoplasma waves in the QPC should not be affected by nonlocal effects at $B > 5$ T, which for the case of the 12th harmonic of the fundamental mode means $X_{12} = 0.32$.

A plasmon selection rule $k_j = \pi j/W$ ($j = 1,2,3,\ldots$) is assumed in the analysis, although the theory for an ungated 2DEG stripe with a constant width W predicts excitation of odd harmonics only [14]. However, to explain our experimental plasmon dispersion with only odd harmonics a significant contribution of the gated plasmons would have to be taken into account. Due to a lack of gate metallization, there is no reason for gated plasmons to be excited. Therefore, we believe that for a low symmetry of the QPC channel both odd and even plasmon modes are allowed.

By applying a gate voltage to the QPC it should be possible to reduce the width W of the channel in the same way that leads to shrinkage of the constriction. The shrinkage should shift the magnetoplasmon frequency and thus change the position of the resonances on the magnetic-field axis. According to Fig. 3(a), the positions of the magnetoplasmon features do not change with V_g. However, taking into account the QPC's threshold voltage ($V_{\rm th} = -2.8$ V), we can estimate that the channel shrinks by about 160 nm per 1 V of the gate polarization. Then,

the position of the fundamental magnetoplasmon resonance should shift to a lower field by $\Delta B \approx 0.01$ T per 1 V of the gate polarization, an amount which is much smaller than a typical width (0.32 T) of the resonance peaks observed.

IV. CONCLUSIONS

In conclusion, using THz magnetospectroscopy, we have observed cyclotron resonance accompanied by magnetoplasmon resonances in high-mobility CdTe/CdMgTe quantum-well-based samples of different channel geometries. In the samples equipped with grating couplers, a mixed nature of these waves has been revealed by data analysis, which shows that they are neither of a purely gated nor purely ungated type. In the quantum point contact structure, a series of practically ungated magnetoplasmon modes has been observed. In each case, the dispersion relation of plasma oscillations was successfully described within a local approximation of the magnetoconductivity tensor of a two-dimensional electron gas, in spite of the fact that the value of the nonlocal parameter X was as high as 0.25 for the magnetoplasmon modes of the highest order. As discussed in this paper, this result remains in a full agreement with nonlocal calculations, which indicate that for the structures under study, the validity of a local approximation should hold up to $X = 0.32$. Also, an increase of the cyclotron effective mass due to a polaron effect and plasmon-LO phonon interaction influence on the 2DEG screening must be taken into account to properly describe the magnetoplasmon dispersion relations.

ACKNOWLEDGMENTS

We are grateful to Professor M. Grynberg for valuable discussions. The research was partially supported by the National Center of Science (Poland) Projects No. DEC-2011/03/B/ST7/03062 and No. DEC-2012/06/A/ST3/00247, and by a Regional Development Program (Poland) Grant No. WND-RPPK 01.03.00-18-053/12. Support from the Foundation for Polish Science through the International Outgoing Scholarship 2014 (T.W.) and through the International Ph.D. Projects Program cofinanced by the EU European Regional Development Fund is also acknowledged.

APPENDIX

The derivation of Eq. (1) presented below follows Refs. [32,36]. An infinite sheet of a 2DEG is situated on a surface of a semi-infinite semiconductor and is separated from the air by a barrier of a thickness d. A magnetic-field induction vector is normal to the plane of the 2DEG. Based on the Drude model, in a quasistatic approximation, the magnetoplasma dispersion relation gets the form (see, for example, Ref. [37])

$$\frac{2\varepsilon_0\bar{\varepsilon}(k,d)\omega_{\rm mp}}{k} + i\sigma_{xx} = 0, \tag{A1}$$

with $\omega_{\rm mp}$ the resonant magnetoplasma frequency, k the magnetoplasma wave vector, and σ_{xx} the component of longitudinal conductivity; $\bar{\varepsilon}(k,d)$ is the dielectric function, which depends on the thickness of the barrier and the wavelength of a magnetoplasmon. According to Refs. [32,36], an analytical expression for σ_{xx} in a semiclassical limit disregarding the electron-electron interaction is

$$\sigma_{xx} = i\frac{4n_s e^2\omega_{\rm mp}}{m^* X^2}\sum_{l=1}^{\infty}\frac{l^2 J_l^2(X)}{\omega^2 - (l\omega_c)^2}. \tag{A2}$$

Here n_s represents a 2DEG concentration, m^* stands for the electron effective mass, $X = kR_c$ (R_c is the electron cyclotron radius), and $J_l(X)$ is a Bessel function of the first kind and the order l. The latter equation assumes a collisionless limit; we use it because we are interested only in a dispersion which relates resonant magnetoplasma frequencies with their wave vectors. Substituting Eq. (A2) with (A1), we get a general dispersion relation for magnetoplasmons,

$$1 - \frac{4\omega_p^2(k,d)}{X^2}\sum_{l=1}^{\infty}\frac{l^2 J_l^2(X)}{\omega^2 - (l\omega_c)^2} = 0, \tag{A3}$$

where $\omega_p^2(k,d) = n_s e^2 k/2\varepsilon_0\bar{\varepsilon}(k,d)m^*$ is a plasmon frequency at zero magnetic field.

A plasmon-LO phonon interaction is introduced by replacing the static dielectric function $\bar{\varepsilon}(k,d)$ in the denominator of $\omega_p(k,d)$ with that depending on the frequency:

$$\bar{\varepsilon}(k,d,\omega) = \bar{\varepsilon}_\infty(k,d)\frac{\omega^2 - \omega_{\rm LO}^2}{\omega^2 - \omega_{\rm TO}^2}. \tag{A4}$$

$\bar{\varepsilon}(k,d)_{b,\infty}$ is the high-frequency dielectric function, and $\omega_{\rm TO}$ and $\omega_{\rm LO}$ are the frequencies of transverse and longitudinal optical phonons, respectively. After putting Eq. (A4) into the denominator of $\omega_p^2(k,d)$, substituting the resulting expression with Eq. (A3), and some trivial mathematical manipulations, we arrive at Eq. (1).

[1] S. J. Allen, Jr., D. C. Tsui, and R. A. Logan, Phys. Rev. Lett. **38**, 980 (1977).
[2] T. N. Theis, J. P. Kotthaus, and P. J. Stiles, Solid State Commun. **24**, 273 (1977).
[3] U. Mackens, D. Heitmann, L. Prager, J. P. Kotthaus, and W. Beinvogl, Phys. Rev. Lett. **53**, 1485 (1984).
[4] J. Alsmeier, E. Batke, and J. P. Kotthaus, Phys. Rev. B **40**, 12574 (1989).
[5] E. Batke, D. Heitmann, and C. W. Tu, Phys. Rev. B **34**, 6951 (1986).
[6] N. Okisu, Y. Sambe, and T. Kobayashi, Appl. Phys. Lett. **48**, 776 (1986).
[7] R. Krahne, M. Hochgräfe, C. Heyn, D. Heitmann, M. Hauser, and K. Eberl, Phys. Rev. B **62**, 15345 (2000).
[8] H. Saxena, R. E. Peale, and W. R. Buchwald, J. Appl. Phys. **105**, 113101 (2009).
[9] N. Nader Esfahani, R. E. Peale, W. R. Buchwald, C. J. Fredricksen, J. R. Hendrickson, and J. W. Cleary, J. Appl. Phys. **114**, 033105 (2013).

[10] A. El Fatimy, S. B. Tombet, F. Teppe, W. Knap, D. B. Veksler, S. Rumyantsev, M. S. Shur, N. Pala, R. Gaska, Q. Fareed, X. Hu, D. Seliuta, G. Valusis, C. Gaquiere, D. Theron, and A. Cappy, Electron. Lett. **42**, 1342 (2006).
[11] A. V. Muravjov, D. B. Veksler, V. V. Popov, O. V. Polischuk, N. Pala, X. Hu, R. Gaska, H. Saxena, R. E. Peale, and M. S. Shur, Appl. Phys. Lett. **96**, 042105 (2010).
[12] K. Nogajewski, J. Łusakowski, W. Knap, V. V. Popov, F. Teppe, S. L. Rumyantsev, and M. S. Shur, Appl. Phys. Lett. **99**, 213501 (2011).
[13] E. Vasiliadou, G. Müller, D. Heitmann, D. Weiss, K. von Klitzing, H. Nickel, W. Schlapp, and R. Lösch, Phys. Rev. B **48**, 17145 (1993).
[14] S. A. Mikhailov and N. A. Savostianova, Phys. Rev. B **71**, 035320 (2005).
[15] I. V. Kukushkin, V. M. Muravev, J. H. Smet, M. Hauser, W. Dietsche, and K. von Klitzing, Phys. Rev. B **73**, 113310 (2006).
[16] V. M. Muravev, C. Jiang, I. V. Kukushkin, J. H. Smet, V. Umansky, and K. von Klitzing, Phys. Rev. B **75**, 193307 (2007).
[17] I. Baskin, B. M. Ashkinadze, E. Cohen, and L. N. Pfeiffer, Phys. Rev. B **84**, 041305 (2011).
[18] M. Białek, M. Czapkiewicz, J. Wróbel, V. Umansky, and J. Łusakowski, Appl. Phys. Lett. **104**, 263514 (2014).
[19] M. Białek, A. M. Witowski, M. Orlita, M. Potemski, M. Czapkiewicz, J. Wróbel, V. Umansky, M. Grynberg, and J. Łusakowski, J. Appl. Phys. **115**, 214503 (2014).
[20] M. Czapkiewicz, V. Kolkovsky, P. Nowicki, M. Wiater, T. Wojciechowski, T. Wojtowicz, and J. Wróbel, Phys. Rev. B **86**, 165415 (2012).
[21] B. A. Piot, J. Kunc, M. Potemski, D. K. Maude, C. Betthausen, A. Vogl, D. Weiss, G. Karczewski, and T. Wojtowicz, Phys. Rev. B **82**, 081307 (2010).
[22] S. D. Ganichev, S. A. Tarasenko, V. V. Bel'kov, P. Olbrich, W. Eder, D. R. Yakovlev, V. Kolkovsky, W. Zaleszczyk, G. Karczewski, T. Wojtowicz, and D. Weiss, Phys. Rev. Lett. **102**, 156602 (2009).
[23] P. Olbrich, C. Zoth, P. Lutz, C. Drexler, V. V. Bel'kov, Y. V. Terent'ev, S. A. Tarasenko, A. N. Semenov, S. V. Ivanov, D. R. Yakovlev, T. Wojtowicz, U. Wurstbauer, D. Schuh, and S. D. Ganichev, Phys. Rev. B **86**, 085310 (2012).
[24] R. Rungsawang, F. Perez, D. Oustinov, J. Gómez, V. Kolkovsky, G. Karczewski, T. Wojtowicz, J. Madéo, N. Jukam, S. Dhillon, and J. Tignon, Phys. Rev. Lett. **110**, 177203 (2013).
[25] Y. Imanaka, T. Takamasu, G. Kido, G. Karczewski, T. Wojtowicz, and J. Kossut, Physica B: Condens. Matter **256-258**, 457 (1998).
[26] G. Karczewski, T. Wojtowicz, Y. Wang, X. Wu, and F. Peeters, Phys. Status Solidi B **229**, 597 (2002).
[27] A. A. Dremin, D. R. Yakovlev, A. A. Sirenko, S. I. Gubarev, O. P. Shabelsky, A. Waag, and M. Bayer, Phys. Rev. B **72**, 195337 (2005).
[28] B. Jusserand, G. Karczewski, G. Cywiński, T. Wojtowicz, A. Lemaître, C. Testelin, and C. Rigaux, Phys. Rev. B **63**, 161302 (2001).
[29] M. Szot, K. Karpierz, J. Kossut, and M. Grynberg, Phys. Status Solidi C **0**, 609 (2003).
[30] M. Szot, K. Karpierz, J. Kossut, and M. Grynberg, AIP Conf. Proc. **772**, 1129 (2005).
[31] I. Grigelionis, M. Białek, M. Grynberg, M. Czapkiewicz, V. Kolkovski, M. Wiater, M. Wojciechowski, J. Wróbel, T. Wojtowicz, N. Diakonova, W. Knap, and J. Łusakowski, Proc. SPIE **9199**, 91990G (2014).
[32] K. Nogajewski, Ph.D. thesis, University of Warsaw, 2013, https://depotuw.ceon.pl/handle/item/310
[33] B. B. Varga, Phys. Rev. **137**, A1896 (1965).
[34] F. Stern, Phys. Rev. Lett. **18**, 546 (1967).
[35] D. V. Fateev, V. V. Popov, and M. S. Shur, Semiconductors **44**, 1406 (2010).
[36] K. W. Chiu and J. J. Quinn, Phys. Rev. B **9**, 4724 (1974).
[37] T. Ando, A. B. Fowler, and F. Stern, Rev. Mod. Phys. **54**, 437 (1982).